

Influence of Cl⁻ on the Initial Corrosion of Weathering Steel in Simulated Marine-Industrial Atmosphere

Libo Wang^{1,2}, Jihui Wang^{1,2,*}, Wenbin Hu²

¹State Key Laboratory of Hydraulic Engineering Simulation and Safety, Tianjin University, Tianjin 300072, P R China

²Tianjin Key Laboratory of Composite and Functional Materials, School of Materials Science and Engineering, Tianjin University, Tianjin 300072, P R China

*E-mail: jhwang@tju.edu.cn

Received: 19 April 2018 / Accepted: 1 June 2018 / Published: 5 July 2018

Influence of Cl⁻ on the initial corrosion of weathering steel in simulated marine-industrial atmosphere was investigated in this paper. The marine-industrial atmospheric corrosion of Q355GNH weathering steel was simulated by the wet/dry cyclic corrosion test in different NaCl + NaHSO₃ solution. The morphology and composition of rust layer on the surface of weathering steel after 30 h test were characterized by SEM and XRD. At the same time electrochemical measurements were conducted to evaluate the corrosion resistance of bare and rusted steel. The result shows that the corrosion rate of weathering steel gradually increases with the increase of Cl⁻ concentration, but the corrosion rate of weathering steel decreases with the formation of rust layer. The compositions of rust layer include lepidocrocite, goethite and magnetite/maghemite. As the concentration of Cl⁻ increases, the content of lepidocrocite and magnetite/maghemite gradually increases while the content of goethite gradually decreases. Meanwhile, the rust layer on the surface of weathering steel becomes less compact.

Keywords: Atmospheric corrosion, weathering steel, rust layer, costal-industrial, electrochemical impedance.

1. INTRODUCTION

Atmospheric corrosion of steel is a complicated problem due to the diversity of atmospheric environment. According to the type and level of pollutions in the air, atmospheric corrosion can be divided into rural, marine, industrial atmospheres and so on [1-3]. The study of atmospheric corrosion is essential because atmospheric corrosion widely exists indoor and outdoor, and causes a lot of economic loss. In these studies, one of the most important focuses is on the influence of different pollutions like sulfur dioxide (SO₂) and chloride on the atmospheric corrosion behavior of steel. In the

past few decades, many researches on the influence of different pollutions were conducted all over the world [4-6].

Chloride is one of the most significant pollutions in marine atmosphere which plays a great role in the corrosion process of steel. At marine atmospheres with a relatively low chloride deposition rate, a consolidated rust layer can be formed on the surface of carbon steel, which can inhibit the penetration of corrosive species (oxygen, water and chloride) to the underlying steel [7,8]. The corrosion rate of steel is dependent on the concentration of chloride and the compositions of rust layer are lepidocrocite, goethite and some magnetite. And akaganeite is another common composition of rust layer that only exists in high salinity environment [9, 10]. However, some researches show that chloride at a certain concentration also can reduce the corrosion rate of steel in atmosphere environment [11].

In industrial atmosphere, sulfur dioxide has the most significant effect on the atmospheric corrosion of steel. And the principal source of sulfur dioxide in industrial atmosphere is the burning of fossil fuels and the emission of exhaust gas from vehicles and factories. Sulfur dioxide has a very high solubility in water and causes acidification of aqueous solutions. In industrial atmosphere including SO_2 and O_2 , iron can be corroded into FeSO_4 . Then FeSO_4 can be oxidized to rust and free H^+ and SO_4^{2-} . This cyclic process can accelerate the corrosion process of steel [12, 13]. But the acceleration effect of SO_2 is not obvious in the initial corrosion stage [14]. And the corrosion rate of steel firstly increase and then decrease with the increase of SO_2 content in atmosphere. Besides, sulfur dioxide can inhibit the formation of $\gamma\text{-FeOOH}$ and promote the formation of $\alpha\text{-FeOOH}$ [15, 16].

With the development of economy, many cities near the costal lines begin to suffer the pollution of industrial exhaust gas, thus the atmosphere has been change to marine-industrial atmosphere. In marine-industrial atmosphere, chloride and SO_2 may have synergistic effect to the corrosion of steel, which leads to more serious corrosion of steel than in marine or industrial atmosphere [17, 18]. But the influence of chloride and SO_2 to the corrosion of weathering steel in marine-industrial atmosphere has not been comprehensively studied. The purpose of this work was to investigate the influence of Cl^- to the initial corrosion of weathering steel in marine-industrial atmosphere by the wet/dry cyclic corrosion test which is a laboratory acceleration method to study atmospheric corrosion of steel.

2. EXPERIMENTAL

2.1. Specimen preparation

The chemical composition of Q355GNH weathering steel is: 0.10 C (in mass%), 0.42 Si, 0.46 Mn, 0.10 P, 0.007 S, 0.32 Cu, 0.55 Cr, 0.29 Ni and Fe, balance. The specimens were prepared to two sizes of 10 mm × 10 mm × 3 mm for electrochemical measurement and 40 mm × 50 mm × 3 mm for weight loss measurement. The samples were mechanically ground successively with 200, 500, 1000 and 2000 grit emery paper before the experiments, and then rinsed with distilled water and absolute ethanol. All samples were reserved in a desiccator before the following tests.

2.2. Wet/dry cyclic corrosion test

The wet/dry cyclic corrosion test involved two stages, together forming one cycle: (1) immersion of samples in NaCl + NaHSO₃ solution for 10 min; (2) exposure in air at room temperature for 50 min. The wet/dry cyclic corrosion test lasted 30 hours, but the samples were taken out after 10, 20 and 30 hours for weight gain measurement. The above solutions were prepared by using analytical grade NaCl and NaHSO₃ and distilled water. Samples used in the test were numbered 1a, 1b, 2a, 2b and so forth. For example, sample 1a was a bare steel and sample 1b was a rusted steel in solution 1. Solutions and corresponding samples and concentrations of NaCl and NaHSO₃ were shown in Table 1.

Table 1. Solutions and corresponding samples and concentrations of NaCl and NaHSO₃ (mol/L)

Solution	Sample	NaCl (mol/L)	NaHSO ₃ (mol/L)
1	1a, 1b	0	0.05
2	2a, 2b	0.01	0.05
3	3a, 3b	0.03	0.05
4	4a, 4b	0.05	0.05

2.3. Characterizations

The weights of weathering steel before the test and after different time wet/dry cyclic corrosion test were measured with an electronic balance. After 30 h test, the rust on the steel surfaces was removed mechanically and chemically in a solution of hydrochloric acid and hexamethylenetetramine (corrosion inhibitor) for 10 min according to international standard of ISO 8407. The steels were then cleaned and dried and weighed again on an electronic balance with an accuracy of 0.1 mg to determine their mass loss.

After 30 h wet/dry cyclic corrosion test in different solutions, the macro morphologies of the surface of rusted steel were observed using an optical microscope (OM). Scanning electron microscopies (SEM) measurements for micro morphology of the cross-section and surface of rusted steel were carried out with a S4800 microscope (Hitachi Limited, Japan) at 5 kV accelerated voltage. The SEM images can stand for the evolution of the rust layer.

The atmospheric corrosion products on the weathering steel were analyzed by X-ray diffraction techniques. Powdered rust was scraped from the rusted steel surface using a razor blade and the powdered rust was characterized by means of X-ray diffraction (XRD) to determine its phases. The XRD data was collected over a 2θ range of 10-80° with a step size of 0.02°.

2.4. Electrochemical measurements

In order to evaluate the corrosion resistance of weathering steel, the polarization curves and electrochemical impedance spectroscopy (EIS) measurements were conducted using an electrochemical workstation with a three electrode system. The bare and rusted specimens with an exposed area of 1 cm² were the working electrodes, a platinum plate was the counter electrode and

Ag/AgCl electrode was the reference electrode. The potentiodynamic polarization curves were conducted on Autolab 302 electrochemical workstation at a sweep rate of 1 mV/s in the over-potential range of ± 250 mV vs. open circuit potential (OCP). The corrosion potential (E_{corr}) and corrosion current density (I_{corr}) were calculated based on the potentiodynamic polarization curves. The impedance spectra were obtained after equilibration in solution for 1 hour when the open circuit potentials of the electrodes became steady. Each impedance spectrum was measured under excitation of a sinusoidal wave with amplitude of 10 mV and the frequency range for EIS was from 10^5 Hz to 0.1 Hz. The impedance spectra were fitted using the ZSimpWin software and the values of fitting parameters were determined by the simulation.

3. RESULTS AND DISCUSSION

3.1. Corrosion kinetics

Weight gain curves of weathering steel in different solutions are shown in Figure 1. And it can be seen that weathering steels in all solutions have a high corrosion rate at the beginning of the wet/dry cyclic corrosion test. And then the corrosion rate of weathering steels gradually decreases with the progress of corrosion.

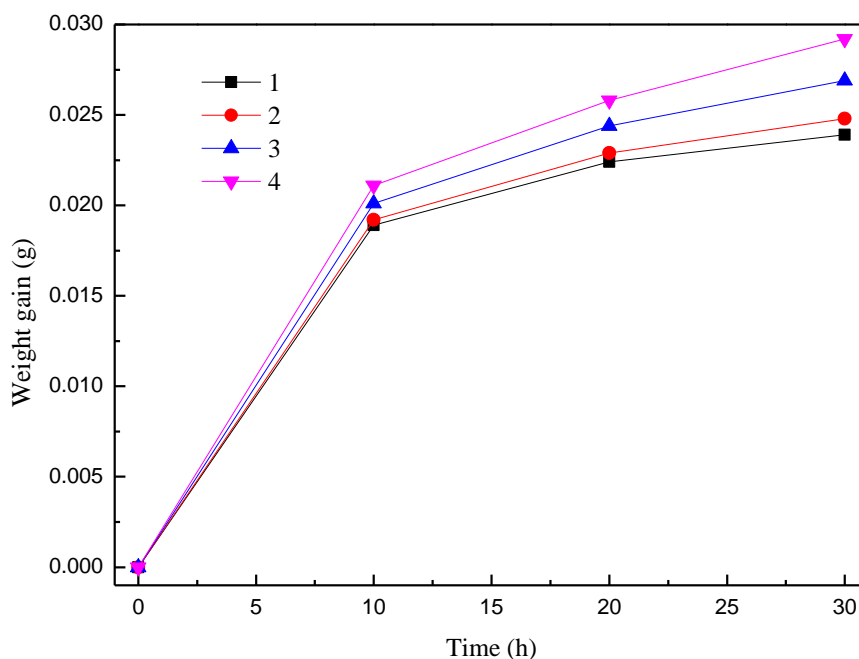


Figure 1. Weight gain curves of weathering steel in different solutions, (1) 0.05 mol/L NaHSO₃, (2) 0.05 mol/L NaHSO₃ + 0.01 mol/L NaCl, (3) 0.05 mol/L NaHSO₃ + 0.03 mol/L NaCl, (4) 0.05 mol/L NaHSO₃ + 0.05 mol/L NaCl.

As the concentration of NaCl increases, the weight gain of weathering steel increases too. It indicates that the increase of NaCl concentration accelerated the corrosion of weathering steel. The weight loss of weathering steels in four solutions after 30 h test was respectively 0.0409, 0.0431, 0.0466, 0.0489 g. According to the weight loss, the corrosion rate of weathering steels can be calculated in Figure 2 by using the following formula:

$$R = \frac{K\Delta m}{St\rho}$$

Where R is the corrosion rate (mm/a), K is an unit constant, Δm is the weight loss before and after corrosion test (g), S is the surface area of specimen (cm²), t is the corrosion time (h) and ρ is the density of weathering steel (g/cm³). From Figure 2 it can be seen that the corrosion rate of weathering steel gradually increases with the increasing of NaCl concentration.

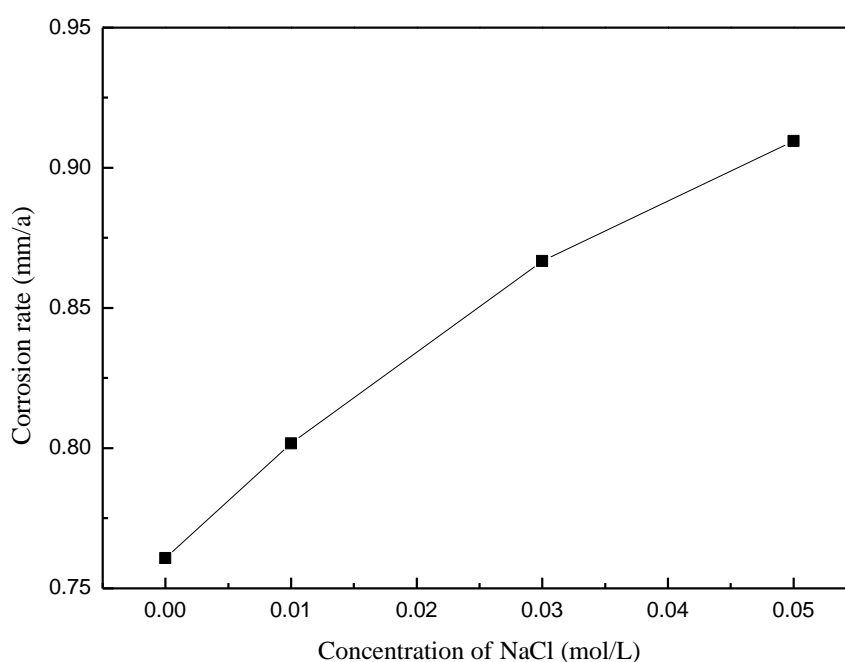


Figure 2. Corrosion rate of weathering steel in different NaCl concentration solutions.

3.2. Morphology of rust layer

Figure 3 shows the macro morphology of rusted steel in four different solutions after 30 h wet/dry cyclic corrosion test. A yellow corrosion products layer with many cracks and holes forms in all weathering steels, and the rust layer become less compact with the increase of NaCl concentration. Figure 4 and Figure 5 present the SEM images for the cross-section and surface of rusted steel in four different solutions. In Figure 4, the bright part of upper layer is epoxy resin, the middle layer is the rust layer and the bottom layer is weathering steel substrate. It can be seen that the compactness of rust layer became poor as the concentration of NaCl increases. And the number of cracks and holes increase especially in the external rust layer, which make the penetration of corrosive species like oxygen easier. In Figure 5, there are many globular formations in the rust layer which are considered to

be goethite. And in high NaCl concentration solutions, some needle-like appearances which is the typical morphology of lepidocrocite can be observed in Figure 5-(4) [19, 20]. The results show that the amount of lepidocrocite increases and the amount of goethite decrease as NaCl concentration increases. But goethite still is the major ingredient in the rust layer. It indicates that Cl^- can promote the formation of lepidocrocite and reduce the compactness of rust layer. But HSO_3^- can promote the transformation of lepidocrocite into goethite, so goethite still is the main composition of rust layer.

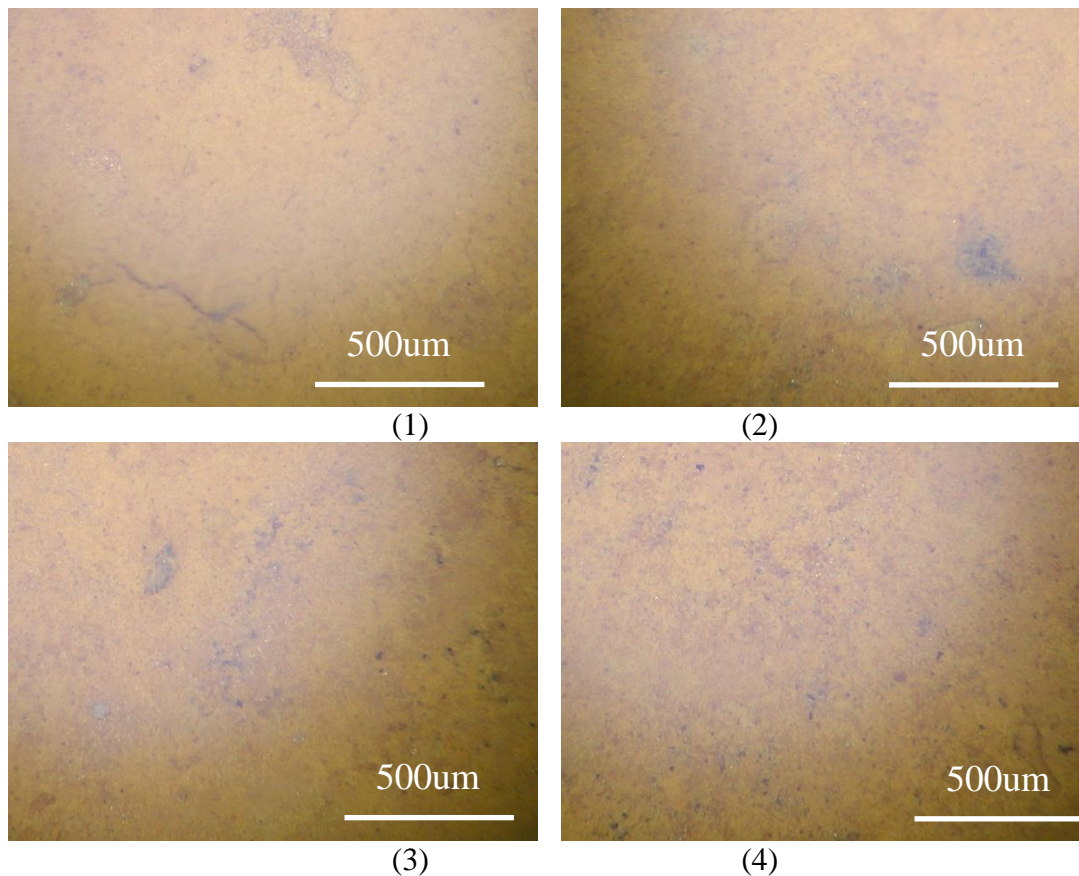
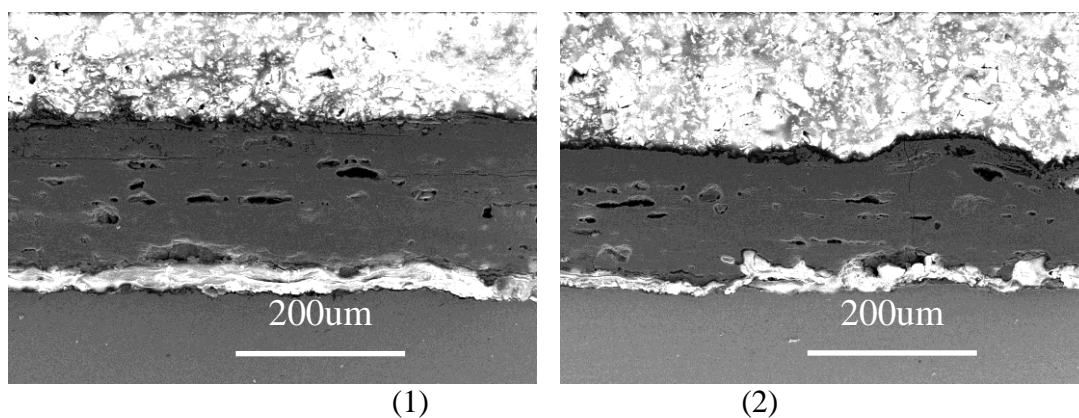


Figure 3. Macro morphology of rusted steel surface in different solutions, (1) 0.05 mol/L NaHSO_3 , (2) 0.05 mol/L NaHSO_3 + 0.01 mol/L NaCl , (3) 0.05 mol/L NaHSO_3 + 0.03 mol/L NaCl , (4) 0.05 mol/L NaHSO_3 + 0.05 mol/L NaCl .



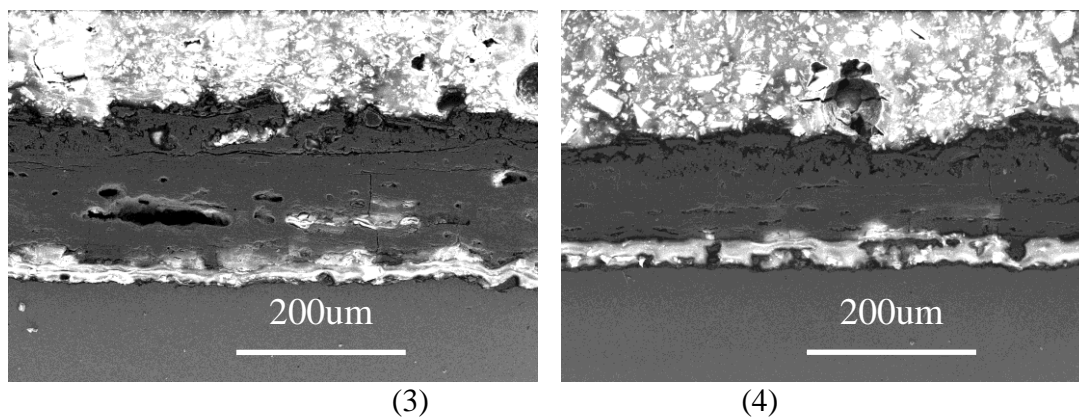


Figure 4. Micro morphology of the cross-section of rusted steel in different solutions, (1) 0.05 mol/L NaHSO₃, (2) 0.05 mol/L NaHSO₃ + 0.01 mol/L NaCl, (3) 0.05 mol/L NaHSO₃ + 0.03 mol/L NaCl, (4) 0.05 mol/L NaHSO₃ + 0.05 mol/L NaCl.

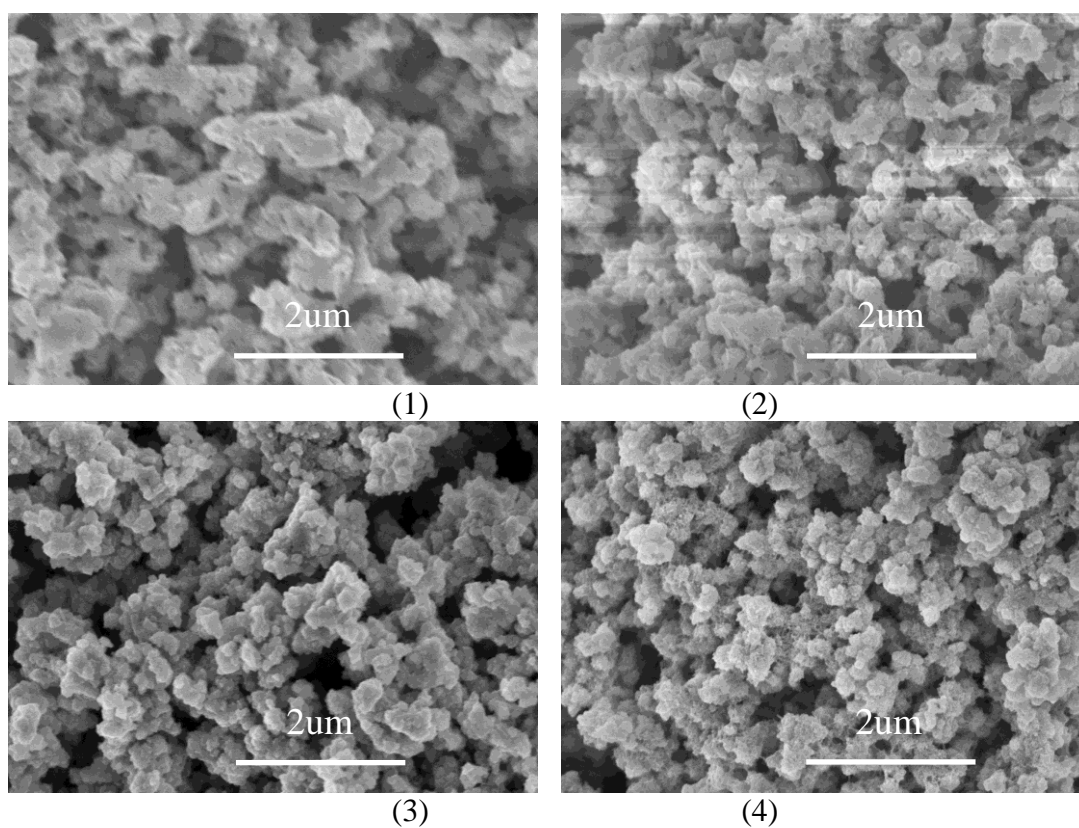


Figure 5. Micro morphology of the surface of rusted steel in different solutions, (1) 0.05 mol/L NaHSO₃, (2) 0.05 mol/L NaHSO₃ + 0.01 mol/L NaCl, (3) 0.05 mol/L NaHSO₃ + 0.03 mol/L NaCl, (4) 0.05 mol/L NaHSO₃ + 0.05 mol/L NaCl.

3.3. XRD

The rust formed on weathering steel in the atmosphere is often composed by several types of iron oxyhydroxides (lepidocrocite and goethite) and iron oxides (magnetite and/or maghemite), which

cannot be separately discerned by XRD method [21]. In particular, amorphous δ -FeOOH (feroxyhyte) is highly abundant in atmospheric corrosion product layers and has been widely reported in the literature [22]. However, XRD only provides a good characterization of crystalline rust. The corrosion products formed on the surface of weathering steel after 30 h wet/dry cyclic corrosion test were characterized by XRD. The results provide a semiquantitative assessment of the crystalline compositions present in the rust layers. Figure 6 displays X-ray diffraction patterns of the rust layer formed in different environment and Figure 7 presents the results of this semiquantification. The result shows that the main constituents of corrosion products formed in NaCl + NaHSO₃ solution are lepidocrocite, goethite and a small amount of magnetite/maghemite. As the concentration of NaCl increases, the relative content of lepidocrocite and magnetite/maghemite gradually increases while the relative content of goethite gradually decreases. This is because that the presence of Cl⁻ can promote the formation of lepidocrocite and inhibit the formation of goethite. But goethite still is the major composition in the rust layer, because the existence of NaHSO₃ makes the aqueous solution acidic, which is benefit to the transformation of lepidocrocite into goethite [23]. This result is consistent with the observed result in SEM images before.

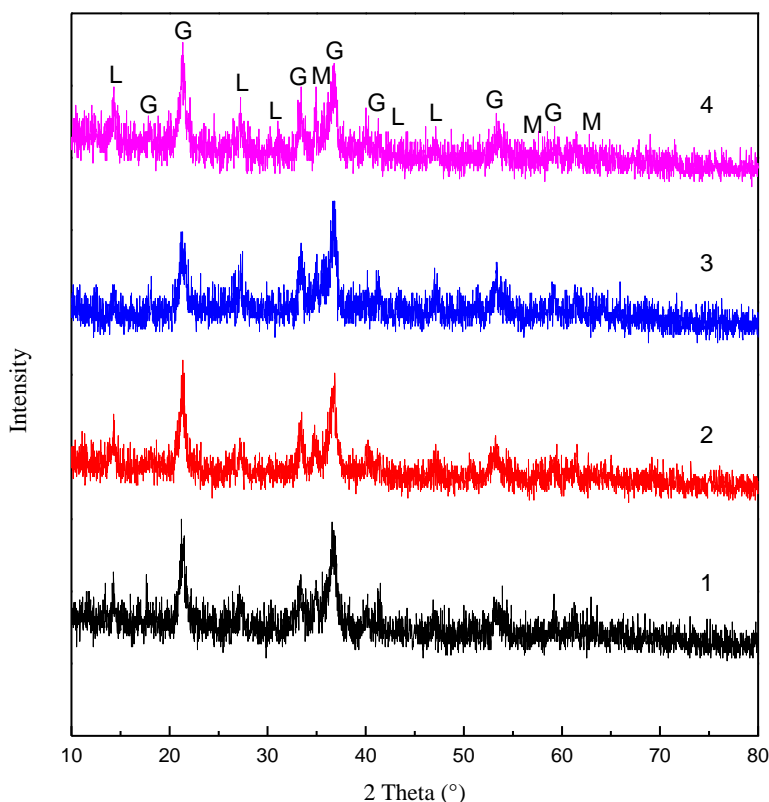


Figure 6. X-ray diffraction patterns of the rust layer after 30 h test in different solutions, (1) 0.05 mol/L NaHSO₃, (2) 0.05 mol/L NaHSO₃ + 0.01 mol/L NaCl, (3) 0.05 mol/L NaHSO₃ + 0.03 mol/L NaCl, (4) 0.05 mol/L NaHSO₃ + 0.05 mol/L NaCl (L = lepidocrocite, G = goethite, M = magnetite and/or maghemite).

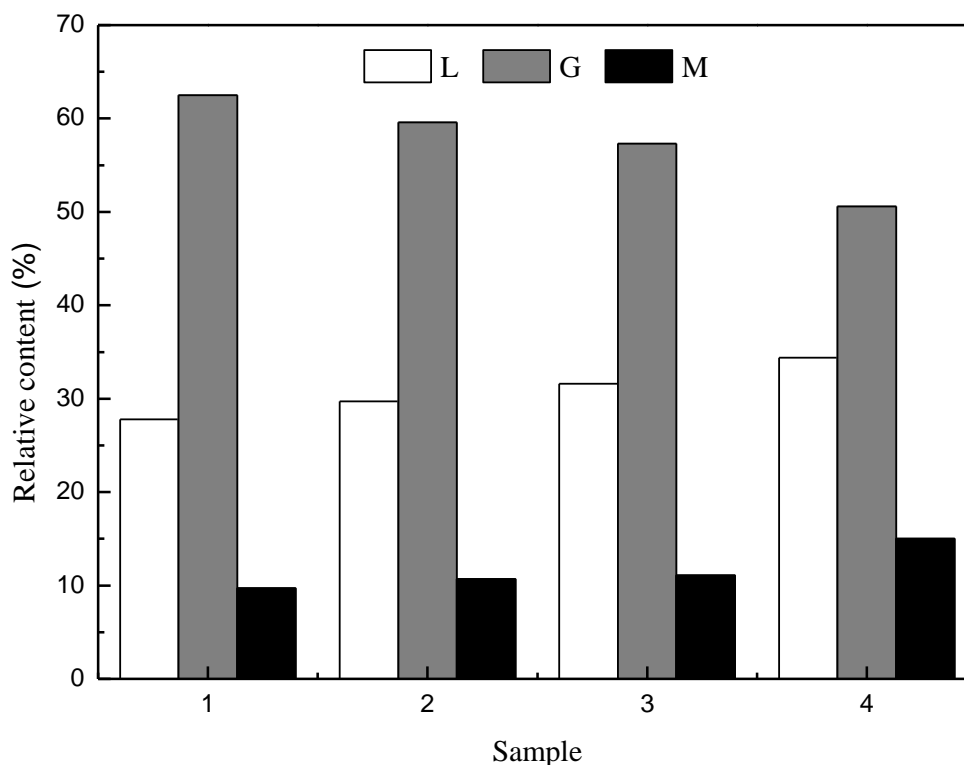


Figure 7. XRD semiquantitative analysis of corrosion products after 30 h test in different solutions, (1) 0.05 mol/L NaHSO₃, (2) 0.05 mol/L NaHSO₃ + 0.01 mol/L NaCl, (3) 0.05 mol/L NaHSO₃ + 0.03 mol/L NaCl, (4) 0.05 mol/L NaHSO₃ + 0.05 mol/L NaCl (L = lepidocrocite, G = goethite, M = magnetite and/or maghemite).

3.4. Polarization curves

The polarization curves of bare and rusted weathering steel in different solutions were shown in Figure 8, and the calculated E_{corr} , I_{corr} , b_a , b_c and R_p of different samples were listed in Table 2. E_{corr} and I_{corr} of bare weathering steel in 0.05 mol/L NaHSO₃ solution were -0.639 V and 322.8 $\mu\text{A}\cdot\text{cm}^{-2}$ respectively. When 0.01 mol/L NaCl was added to the solution, E_{corr} of weathering steel was -0.638 V but I_{corr} of weathering steel had a significant increased to 416.2 $\mu\text{A}\cdot\text{cm}^{-2}$. As the concentration of NaCl increases from 0.01 mol/L to 0.05 mol/L, E_{corr} of steel basically remained constant while I_{corr} of steel increases continually to 481.4 $\mu\text{A}\cdot\text{cm}^{-2}$. It indicates that the corrosion rate of bare weathering steel increases with the increase of NaCl concentration. The anodic Tafel slope gradually increases and the cathodic Tafel slope decreases when the concentration of NaCl increases from 0 to 0.05 mol/L. It may be because the adsorption of Cl⁻ on the surface of weathering steel promotes anodic dissolution of iron and to some extent inhabits the cathodic reaction.

After 30 h wet/dry cyclic corrosion test, E_{corr} of rusted weathering steel in 0.05 mol/L NaHSO₃ solution had a slight decrease to -0.646 V and I_{corr} of weathering steel significantly decreased to 187.4 $\mu\text{A}\cdot\text{cm}^{-2}$. In all other NaCl + NaHSO₃ solutions, I_{corr} of rusted weathering steel have a significant

decline than bare weathering steel. In addition, the anodic and cathodic Tafel slope of rusted weathering steel is lower compared to bare weathering steel in the same solution, because the rust layer hinders the anodic and cathodic reaction. The result shows that the rust layer on the surface of weathering steel possesses a good protection of weathering steel substrate, and decreases the corrosion rate of weathering steel. This is why the weight gain curves of weathering steel in different solutions gradually become flat in Figure 1.

In different solutions, rusted weathering steel have similar E_{corr} , but I_{corr} of rusted weathering steel gradually increases when the concentration of NaCl increases. It indicates that the corrosion rate of rusted weathering steel also increases with the increasing of NaCl concentration. From these results it can be conclude that the increase of NaCl concentration in solution can promote the corrosion of whatever bare weathering steel or rusted weathering steel, and the formation of a protective rust layer on the surface of weathering steel can decrease the corrosion rate of weathering steel [24].

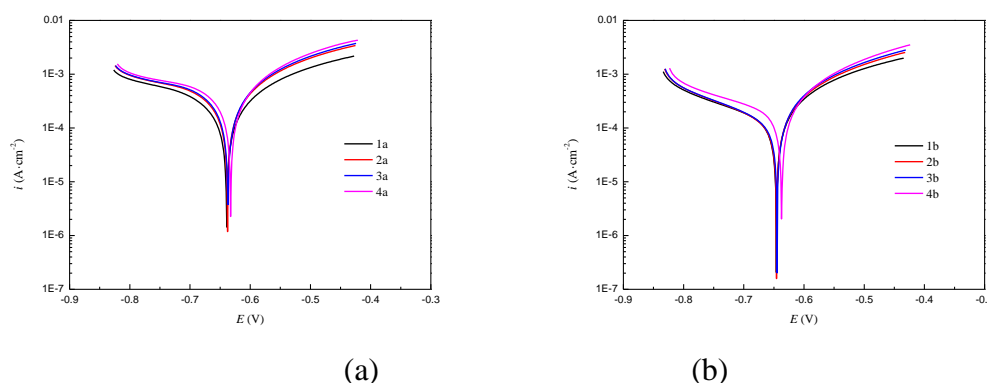


Figure 8. Polarization curves of bare (a) and rusted (b) weathering steel in different solutions, (1) 0.05 mol/L NaHSO₃, (2) 0.05 mol/L NaHSO₃ + 0.01 mol/L NaCl, (3) 0.05 mol/L NaHSO₃ + 0.03 mol/L NaCl, (4) 0.05 mol/L NaHSO₃ + 0.05 mol/L NaCl.

Table 2. E_{corr} , I_{corr} , b_a , b_c and R_p of bare and rusted weathering steel in different solutions

Sample	E_{corr} (V)	I_{corr} ($\mu\text{A}\cdot\text{cm}^{-2}$)	b_a (V/dec)	b_c (V/dec)	R_p ($\Omega\cdot\text{cm}^2$)
1a	-0.639	322.8	0.394	-0.269	142.8
1b	-0.646	187.4	0.235	-0.231	208.2
2a	-0.638	416.2	0.422	-0.241	107.4
2b	-0.645	192.4	0.238	-0.217	191.0
3a	-0.637	446.0	0.457	-0.234	102.1
3b	-0.645	203.3	0.256	-0.206	170.7
4a	-0.632	481.4	0.492	-0.233	90.55
4b	-0.637	253.2	0.292	-0.198	147.9

3.5. Electrochemical impedance spectroscopy

Figure 9 shows Nyquist plots and Bode plots for bare and rusted weathering steel in different NaCl + NaHSO₃ solutions. Nyquist plot of bare weathering steel in different solutions is in only one capacitive impedance arc, and the impedance modulus decrease with the increase of NaCl concentration. After 30 h wet/dry cyclic corrosion test, two capacitive impedance arcs were observed in Nyquist plots of rusted steel, which may be attributed to the formation of rust layer on the surface of steel, and the impedance modulus also decrease with the increase of NaCl concentration.

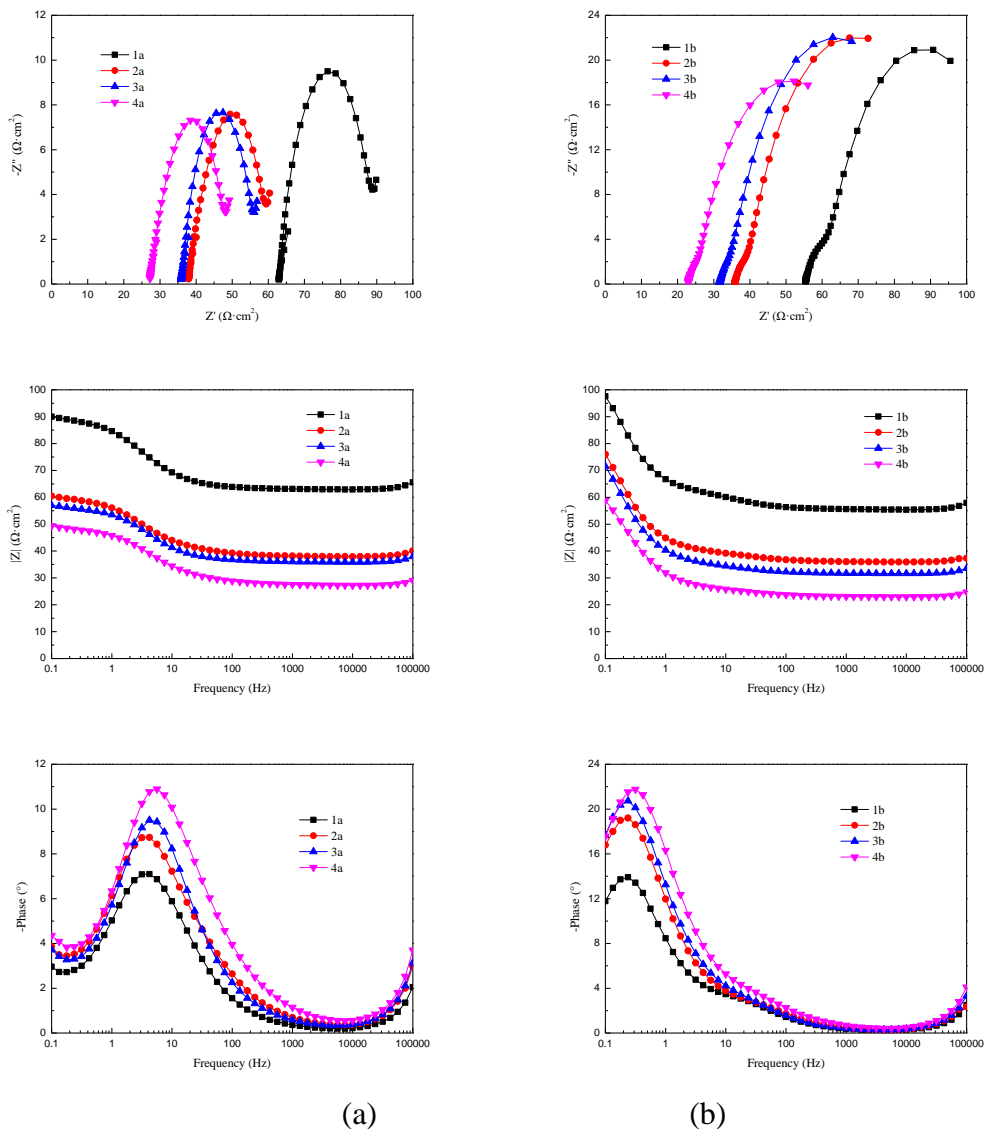


Figure 9. Nyquist plots and Bode plots of bare (a) and rusted (b) weathering steel in different solutions, (1) 0.05 mol/L NaHSO₃, (2) 0.05 mol/L NaHSO₃ + 0.01 mol/L NaCl, (3) 0.05 mol/L NaHSO₃ + 0.03 mol/L NaCl, (4) 0.05 mol/L NaHSO₃ + 0.05 mol/L NaCl.

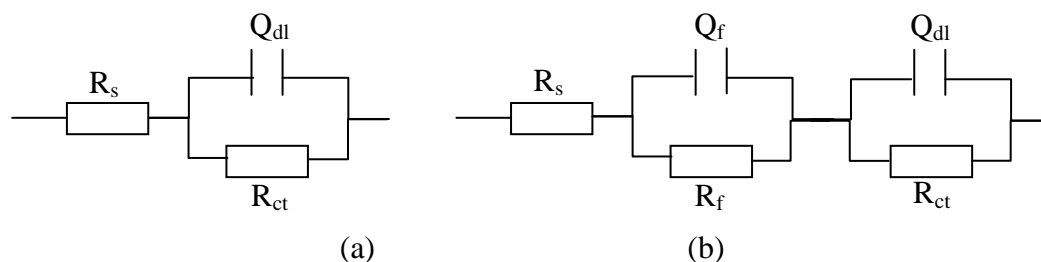


Figure 10. Equivalent circuit of bare (a) and rusted (b) weathering steel in different solutions

Table 3. Fitting results of EIS data for bare (a) and rusted (b) weathering steel in different solutions, (1) 0.05 mol/L NaHSO₃, (2) 0.05 mol/L NaHSO₃ + 0.01 mol/L NaCl, (3) 0.05 mol/L NaHSO₃ + 0.03 mol/L NaCl, (4) 0.05 mol/L NaHSO₃ + 0.05 mol/L NaCl.

Sample	R_s ($\Omega \cdot \text{cm}^2$)	Q_{dl} ($\mu\text{F} \cdot \text{cm}^{-2}$)	α_1	R_{ct} ($\Omega \cdot \text{cm}^2$)	Q_f ($\mu\text{F} \cdot \text{cm}^{-2}$)	α_2	R_f ($\Omega \cdot \text{cm}^2$)
1a	62.9	4109	0.74	28.1			
1b	55.4	20110	0.85	58.5	5450	0.72	7.1
2a	37.9	5975	0.67	24.2			
2b	35.9	21000	0.82	57.4	7782	0.70	4.2
3a	35.9	4660	0.75	23.3			
3b	31.6	21340	0.83	52.4	10440	0.67	3.9
4a	27.2	5028	0.67	21.8			
4b	22.9	21480	0.79	50.4	12600	0.67	2.9

Figure 10 shows the equivalent circuits applied for bare and rusted weathering steel in NaCl + NaHSO₃ solutions, and the corresponding fitting parameters are listed in Table 3 [25]. In Figure 10, R_s represents the solution resistance; R_{ct} is the charge transfer resistance of weathering steel; Q_{dl} is defined as the capacitance of electric double layer of weathering steel; R_f is the resistance of rust layer on steel and Q_f is defined as the capacitance of rust layer. Figure 11 shows Q_f and R_f of rusted weathering steel in different NaCl concentration solutions.

As for bare weathering steel, R_{ct} gradually decreases from 28.1 to 21.8 $\Omega \cdot \text{cm}^2$ when the concentration of NaCl increases from 0 to 0.05 mol/L, which means the corrosion rate of bare weathering steel gradually increase. After 30 h wet/dry cyclic corrosion test, the surface of steel was covered with a rust layer. R_{ct} of rusted steel had a clear increase than that of bare steel.

From above results, it also can be observed that the rust layer forming in NaCl + NaHSO₃ solutions have a good protection to steel and suppress the corrosion of steel. But R_{ct} of rusted steel still gradually decreases with the increase of NaCl. As the concentration of NaCl increases, Q_f increases and R_f decreases for the rusted steel. The reason is that the rust layer of weathering steel became less compact in higher NaCl concentration solution as shown in Figure 5.

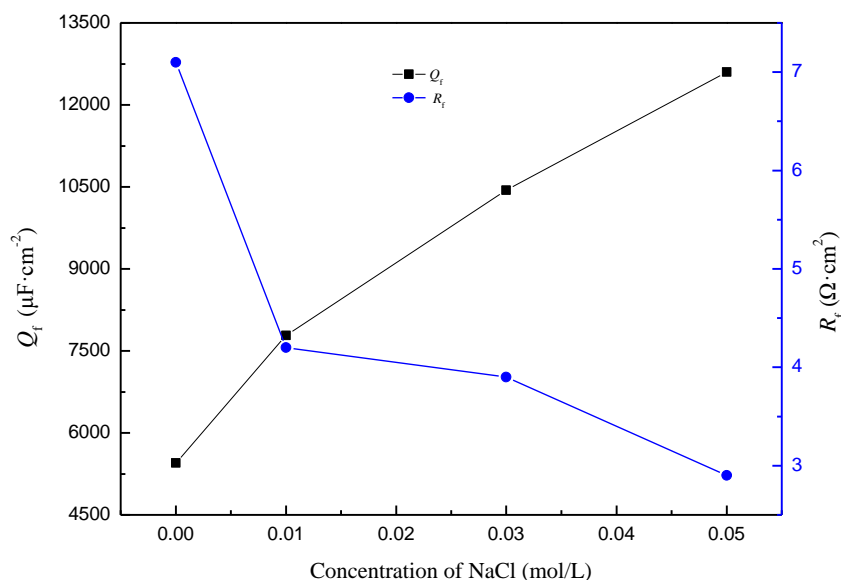


Figure 11. Q_f and R_f of rusted weathering steel in different NaCl concentration solutions

4. CONCLUSIONS

(1) In NaCl + NaHSO₃ solutions, the main compositions of rust layer on weathering steel surface are lepidocrocite, goethite and a small amount of magnetite/maghemite. As the concentration of NaCl increases, the content of goethite decreases while the content of lepidocrocite and magnetite/maghemite increase. And the rust layer become less compact and stable, which makes the protective effect of rust layer to the weathering steel decreases.

(2) Through the weight loss and electrochemical measurements, it can be seen that with the increase of NaCl concentration, the corrosion rate of weathering steel increases. And the corrosion rate of weathering steel decreases with the progress of corrosion. The rust layer on weathering steel surface could inhibit the corrosion of weathering steel. And the corrosion rate of rusted weathering steel also increases with the increase of NaCl concentration.

ACKNOWLEDGMENTS

This paper was supported by National Natural Science Foundation of China (51471117), National Basic Research Program of China (2014CB046801) and Independent Innovation Fund Cooperation Project between Tianjin University and Qinghai University for Nationalities (1706).

References

1. S.J. Oh, D. Cook and H. Townsend, *Corros. Sci.*, 41 (1999) 1687.
2. H.E. Townsend, T. Simpson and G. Johnson, *Corrosion*, 50 (1994) 546.
3. Z. Wang, J. Liu, L. Wu, R. Han and Y. Sun, *Corros. Sci.*, 67 (2013) 1.

4. J. Dong, E. Han and W. Ke, *Sci. Technol. Adv. Mat.*, 8 (2007) 559.
5. D. Singh, S. Yadav and J.K. Saha, *Corros. Sci.*, 50 (2008) 93.
6. Y. Ma, Y. Li and F. Wang, *Corros. Sci.*, 51 (2009) 997.
7. D. de la Fuente, I. Díaz, J. Alcántara, B. Chico, J. Simancas, I. Llorente, A. García-Delgado, J.A. Jiménez, P. Adeva and M. Morcillo, *Mater. Corros.*, 67 (2016) 227.
8. Y. Ma, Y. Li and F. Wang, *Corros. Sci.*, 51 (2009) 1725.
9. M. Yamashita, A. Maeda, H. Uchida, T. Kamimura and H. Miyuki, *J. Jpn. I. Met.*, 65 (2001) 967.
10. T. Nishimura, H. Katayama, K. Noda and T. Kodama, *Corrosion*, 56 (2000) 935.
11. A. Morales, D. Cartagena, J. Rendon and A. Valencia, *Phys. Status. Solidi. B*, 220 (2000) 351.
12. Y. Ma, Y. Li and F. Wang, *Mater. Chem. Phys.*, 112 (2008) 844.
13. J. Wang, F. Wei, Y. Chang and H.C. Shih, *Mater. Chem. Phys.*, 47 (1997) 1.
14. W. Chen, L. Hao, J. Dong and W. Ke, *Corros. Sci.*, 83 (2014) 155.
15. L. Hao, S. Zhang, J. Dong and W. Ke, *Metall. Mater. Trans. A*, 43 (2012) 1724.
16. F.Y. Mi, X.D. Wang, Z.P. Liu, W. Bing, P. Yun and D.P. Tao, *J. Iron. Steel. Res. Int.*, 18 (2011) 67.
17. L. Hao, S. Zhang, J. Dong and W. Ke, *Corros. Sci.*, 59 (2012) 270.
18. I. Allam, J. Arlow and H. Saricimen, *Corros. Sci.*, 32 (1991) 417.
19. D. de la Fuente, J. Alcántara, B. Chico, I. Díaz, J.A. Jiménez and M. Morcillo, *Corros. Sci.*, 110 (2016) 253.
20. A. Raman, S. Nasrazadani and L. Sharma, *Metallography*, 22 (1989) 79.
21. R.A. Antunes, I. Costa and D.L.A.d. Faria, *Materials Research*, 6 (2003) 403.
22. T. Misawa, K. Asami, K. Hashimoto and S. Shimodaira, *Corros. Sci.*, 14 (1974) 279.
23. M. Yamashita, H. Konishi, T. Kozakura, J. Mizuki and H. Uchida, *Corros. Sci.*, 47 (2005) 2492.
24. T. Kamimura, S. Hara, H. Miyuki, M. Yamashita and H. Uchida, *Corros. Sci.*, 48 (2006) 2799.
25. L. Song, X. Ma, Z. Chen and B. Hou, *Corros. Sci.*, 87 (2014) 427.

© 2018 The Authors. Published by ESG (www.electrochemsci.org). This article is an open access article distributed under the terms and conditions of the Creative Commons Attribution license (<http://creativecommons.org/licenses/by/4.0/>).